Communication



# Size-controlled ZnO Nanoparticles Synthesized with Thioacetamide and Formation of ZnS Quantum dots

Ju-Seong Kim , Jonghyun Choi , Won Kook Choi *

Posted Date: 7 September 2023

doi: 10.20944/preprints202309.0472.v1

Keywords: size-controlled ZnO nanoparticles; the formation of ZnS nanoparticles; quantum dots; sol-gel; hydrothermal; ethanolic thioactamide; crystal growth; chemical conversion

*Communication*

# Size-controlled ZnO Nanoparticles Synthesized with Thioacetamide and Formation of ZnS Quantum dots

**Ju-Seong Kim, Jonghyun Choi and Won Kook Choi ***

Center for Opto-Electronic Materials and Devices, Korea Institute of Science and Technology (KIST), Seoul, 02792 Korea

* Correspondence: wkchoi@kist.re.kr; Tel.: +82 2-958-5562

**Abstract:** In this work, we report on the first attempt using size-controlled ZnO nanoparticles (NPs) to analyze role of thioacetamide (TAA) in forming ZnS nanostructures from ZnO. The size-controlled B(blue)_, G(green)_, Y(yellow)_ZnO QDs, and NC (nanocrystalline)_ZnO NPs were synthesized by sol-gel process as well as hydrothermal method, respectively and then reacted with an ethanolic TAA solution as sulfur source. After reacting with TAA, the formation of ZnS QDs was observed over time. The chemical reactions were identified using X-ray diffraction (XRD), Transmission Electron Microscope (TEM), UV-vis spectroscopy, and Photoluminescence (PL). All results indicate that ZnS formation is due to direct crystal growth and/or chemical conversion of ZnO to ZnS. Our results enable a broader understanding of the synthetic mechanisms involved in the use of TAA as a sulfur source in forming ZnS nanostructures from ZnO.

**Keywords:** size-controlled ZnO nanoparticles; the formation of ZnS nanoparticles; quantum dots; sol-gel; hydrothermal; ethanolic thioactamide; crystal growth; chemical conversion

## 1. Introduction

II-VI ZnO semiconductors have received considerable attention because of their advantages such as a wide band gap (3.37 eV), large exciton binding energy (60 meV), high electron mobility (≈205 $cm^2/Vs$), high optical transparency, low toxicity in Vivo, and a low price due to abundance of resources [1–11]. Specifically, ZnO quantum dots (QDs) are a promising material type due to their advantages, such as a size-tunable band gap and electrical properties without altering the composition and a low-cost fabrication technique that is compatible with solution-processed methods [12–16]. Therefore ZnO QDs have been most widely adopted as an electron transport layer (ETL) in photovoltaic cells and light emitting diodes. Despite these many advantages, however, ZnO QDs have difficulty controlling excessive trap levels and structural luminescence weakness in which a direct band edge (band-to-band) emission is rapidly reduced due to surface defects [17,18]. Several studies have demonstrated ways to improve the intrinsic properties of ZnO, including control and design of the point defect structures, as well as surface and interfacial structures [19–26]. More specifically, the ZnO/ZnS nanocomposites is an attractive approach to modify the particle characteristics and properties of ZnO [27,28]. The ZnO/ZnS nanocomposites, such as core-shell QDs, nanorods, nanowire, nanobelt, nanocage, have been successfully prepared using various methods [29–38]. Herein, the shell can acts as a barrier between the shell interior and the surrounding environment, eliminate surface-related defect states, and improve physical and chemical stability. In addition, the photoluminescence properties of the core can be improved by reducing the non-radiative recombination of photogenerated electron-hole pairs [39]. To form ZnO/ZnS nanostructures, $Na_2S$ and thioacetamide (TAA) are commonly used as sulfur sources, whereas few results were reported for nanocomposites using TAA on ZnO. For example, Luo *et al*. have reported Cd-doped ZnO/ZnS core/shell QDs and obtained ZnO/ZnS core/shell QDs with significantly reduced visible emission by TAA [28]. Manaia *et al*. have also obtained ZnO/ZnS heterostructures prepared with different concentration of the sulfur source (TAA) [40]. As these results regarding TAA-induced

 doi:10.20944/preprints202309.0472.v1



ZnS formation have not been clearly interpreted, a special approach is required to better understand them.

In this work, we firstly attempt to use size-controlled ZnO NPs for analyzing the role of TAA in the formation of ZnS nanostructures from ZnO. We prepared samples of the small-sized Y_, G_ and B_ZnO QDs named according to the PL wavelengths such as blue, green, and yellow, and sample of a few tenth nm size NC (nanocrystalline)_ZnO NPs. The samples of the B_, G_, and Y_ZnO QDs were synthesized at low temperatures via a simple sol-gel method, as described in our previous reports [41]. The NC_ZnO NPs were synthesized through hydrothermal method using a zinc acetate dehydrate (ZAD) precursor solution [42]. The size-controlled B_, G_, Y_ZnO QDs, and NC_ZnO NPs were reacted with the same amount of TAA solution and analyzed according to the reaction progress time. Crystalline structure and crystallite size of nanocomposites were characterized by X-ray diffraction (XRD) and Transmission Electron Microscope (TEM). UV-vis spectroscopy, Photoluminescence (PL), and Photoluminescence excitation (PLE) were adopted to further estimate the average particle size and to analyze the optical properties of the ZnO synthesized with/without TAA. During all size-controlled ZnO NPs reacted with TAA, the ZnO NPs were completely consumed and the ZnS QDs were newly formed, regardless of the sizes of ZnO NPs. Our results enable a broader understanding of the synthetic mechanisms involved in the use of TAA as sulfur source in forming ZnO/ZnS nanostructures.

## 2. Materials and Methods

### *2.1. Materials*

ZAD (99.0%), lithium hydroxide (LiOH, 98.0%), N, N-Dimethylformamide (DMF, 99.9), thioacetamide (TAA, 99%), n-hexane, and anhydrous ethanol (EtOH), were purchased from Sigma Aldrich and used without any further purification.

### *2.2. Synthesis of ZnO NPs*

All size-controlled ZnO NPs were prepared using a previously reported similar methods with modifications. The ZnO QDs were synthesized at low temperatures via a simple sol-gel method [41]. Solution of ZAD and LiOH were prepared in EtOH, and stirred at 60°C for 1 day. The LiOH solution was added dropwise to the ZAD solution in a 250 mL flask at 70°C and stirred for 1 h. In order to synthesize B_, G_, and Y_ZnO, LiOH/ZAD solutions with molar ratio of 1.2, 1.6, and 2.16, respectively, were used. The NC_ZnO NPs were synthesized through hydrothermal method using a ZAD solution [42]. The ZAD 0.92 g prepared in 200 mL of DMF were stirred at 110°C for 5 h. The resulting solutions were subjected to further purification by repeating the two-step purification process to remove the residue.

### *2.3. Synthesis of ZnO/ZnS nanocomposites*

The ZnO/ZnS nanocomposites were prepared using a previously reported similar methods with modifications [28,40]. Both 1.317 g of ZAD and 0.3 g of TAA were dissolved in EtOH and stirred at 40°C until fully dissolved. A given amount of the solution and an equal volume of the ZnO solutions were mixed at room temperature under constant stirring. The TAA solution was added to the ZAD solution and B_, G_, Y_ZnO QDs, and NC_ZnO NPs at 40°C for 1 h, respectively. The solutions were repeatedly washed with n-hexane to remove the residue.

### *2.4. Characterization*

X-ray diffraction (XRD) patterns of the samples were recorded using an X-ray diffractometer (Rigaku ATX-G) with Cu K$\alpha$ radiation of wavelength $\lambda$ = 1.5406 Å. Using a transmission electron microscope (TEM, TalosF200X), the morphology, size, and elemental composition of the samples were investigated. TEM samples were prepared by dispersing ZnO dry powders in deionized water or EtOH to form a homogeneous suspension. The size distribution of ZnO samples was analyzed

Preprints (www.preprints.org) | NOT PEER-REVIEWED | Posted: 7 September 2023 doi:10.20944/preprints202309.0472.v1



using TEM Imaging & Analysis software (FEI Co.). UV-Vis absorption data were recorded by a PerkinElmer Lambda 18 UV–vis spectrometer with QS grade quartz cuvettes. PL and PLE data were recorded by a Hitachi F-7000 fluorescence system with QS-grade quartz cuvettes.

## 3. Results and discussions

The chemical reaction of ZnO NPs and ZnS QDs are presented in Scheme 1. After base-catalyzed hydrolysis and condensation reactions from ZAD precursors to ZnO particles, as shown in reaction (1) [43–45], TAA solution used as a sulfur source was then added to the size-controlled ZnO NPs, as shown in reaction (2), respectively. The TAA, used as a sulfur source, can be induced the conversion of ZnO to ZnS by complex and many chemical reaction. When acetate moieties in ethanolic ZAD solutions are released, acetic acid, esters or additional water can be formed reacting with ethanol. TAA can be decomposed by water formed from ZAD, releasing acetamide and S ions. Here, with a sufficient amount of TAA, full chemical conversion of ZnO to ZnS could be expected according to their respective solubility constants. [28,40,43,46].

$$ZnAc_2 \cdot 2H_2O \xrightarrow[\text{ZAD}]{\triangle} AcO-Zn-OAc \xrightarrow{OH^-} HO-Zn-OH + HO-Zn-OH \longrightarrow HO-Zn-O-Zn-OH \longrightarrow ZnO_{(s)} \quad (1)$$

$$CH_3CSNH_2 + H_2O \xrightarrow[\text{TAA}]{} CH_3CONH_2 + H_2S$$

$$Zn^{2+} + H_2S \longrightarrow ZnS_{(s)} + 2H^+ \quad (2)$$

$$ZnAc_2 \cdot 2H_2O \xrightarrow[LiOH \cdot H_2O]{} \text{ZnO} \xrightarrow[TAA]{ZnAc_2 \cdot 2H_2O} \text{ZnS}$$

**Scheme 1.** Schematic illustration of the synthesis of ZnO and ZnS QDs.

Figure 1 presents the XRD patterns of ZnO samples synthesized without TAA and with TAA for 1 h. The ZnO had a hexagonal wurtzite structure with diffraction peaks of (100), (002), (101), (102), (110), (103), and (112) crystalline planes and the ZnS had a cubic zinc blende structure with diffraction peaks of (111), (220), and (311) crystalline planes. The positions of XRD patterns of the ZnO are marked with dashed black lines while those indicative of the ZnS are marked with dashed red lines. Absence of impurity peaks can be expected for high purity of the sample. Here, all diffraction peaks of the ZnO samples synthesized without TAA are in good agreement with those of hexagonal wurtzite ZnO (PDF No. 36-1451). The narrowing of peaks in the diffraction patterns of all the synthesized products clearly indicates the formation of big-sized NCs from small-sized QDs. In the case of the NC_ZnO NPs, which shows relatively clear grain crystal characteristics, the average size of particles could be estimated using the Debye–Scherrer relation and the crystallite sizes were about 45 nm [47]. Whereas, all diffraction peaks of the ZnO samples synthesized with TAA is consistent of the ZnS phase (PDF No. 05-0566). For the ZnO NPs synthesized with TAA for 1 h, the remarkable XRD patterns of ZnO has not been identified. These results indicate that the wurtzite ZnO particles synthesized with TAA can be consumed and the cubic zinc blende ZnS formed [40].

Preprints (www.preprints.org) | NOT PEER-REVIEWED | Posted: 7 September 2023 doi:10.20944/preprints202309.0472.v1



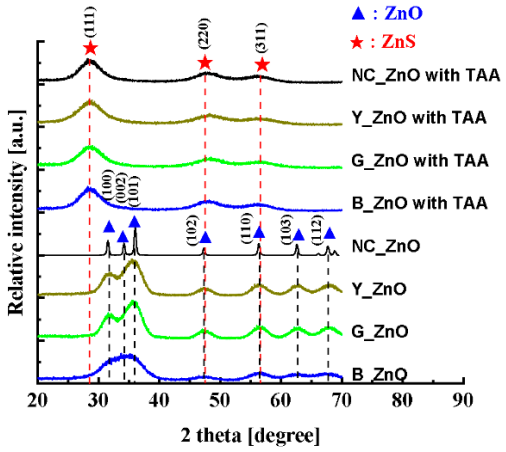


**Figure 1.** XRD patterns for ZnO QDs with/without TAA. (a) B_ZnO QDs, (b) G_ZnO QDs, (c) Y_ZnO QDs, and (d) NC_ZnO NPs.

TEM images of the ZnO samples synthesized without TAA and the ZnO samples synthesized with TAA are presented in Figure 2. As is apparent from Figure 2(top), B_, G, and Y_ZnO QDs synthesized without TAA present approximately spherical shapes with approximate diameter of about 2.6, 2.9, and 3.2 nm, respectively. It is noteworthy that G_ and Y_ZnO QDs well dispersed whereas the B_ZnO QDs are agglomerated because of their high surface energy. The NC_ZnO NPs synthesized without TAA present approximately distorted hexagonal shapes with approximate diameter of more than 40 nm which agrees well with the calculated value of about 45 nm using Debye-Scherrer equation in XRD. On the other hand, the B_, G_, Y_ZnO QDs, and NC_ZnO NPs synthesized with TAA finally vanished, and only spherical ZnS QDs with similar diameters of 2.2 nm were observed in all samples, as shown in Figure 2(bottom). Here, the NC_ZnO with the largest was consumed without trace, as shown in Figure 2(inset). This can be interpreted as the consumption of the ZnO regardless of the particle size with the simultaneous formation of ZnS QDs [40] and is in good agreement with our XRD results.

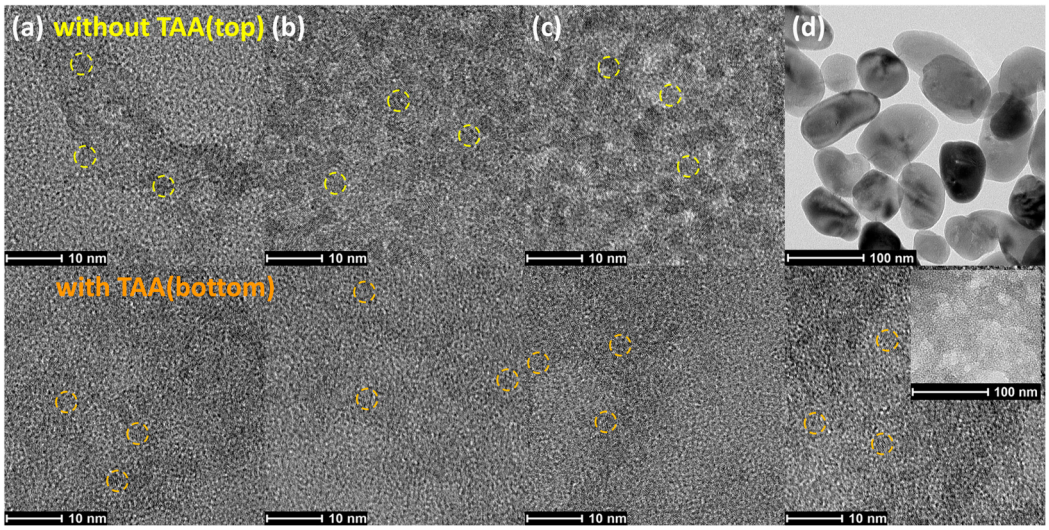


**Figure 2.** TEM images for ZnO synthesized without TAA (top) and with TAA (bottom). (a) B_ZnO QDs, (b) G_ZnO QDs, (c) Y_ZnO QDs, and (d) NC_ZnOs (Inset shows low-magnification of TEM images).

UV-Vis absorption spectra of different reaction times with/without TAA are presented in Figure 3. With decreasing particle size, a blue-shift of excitonic absorption and an increase of band gap are

Preprints (www.preprints.org) | NOT PEER-REVIEWED | Posted: 7 September 2023 doi:10.20944/preprints202309.0472.v1



well-known characteristics of QDs. In the absorption spectra, the difference for the particle size of B_, G_, Y_, and NC_ZnOs are clearly observed, respectively. The B_, G_, Y_ZnO QDs, and NC_ZnO NPs synthesized without TAA exhibited the absorption peak at 297, 322, 333, and 370 nm, respectively. According to the equation reported by Meulenkamp [48], the particle size the ZnO QDs except for NC_ZnO NPs can be estimated at the measured absorption wavelengths as much as 2.6, 3.2, and 3.5 nm for B_, G_, and Y_ZnO QDs, respectively, which is consistent with the results measured from TEM. No dramatic change in ZnO particle size was observed as the reaction proceeds with TAA. In the absorption spectra of B_ZnO QDs, after synthesizing for 5 min with TAA a new absorption peak at 266 nm except the peak at 322 nm newly occurred which indicates that the new material was formed. And then the peak at 322 nm completely disappeared after synthesizing for 10 min with TAA and a new broad peak at around 290 nm additionally appeared. The excitonic peaks at about 266 nm and 290 nm are well-known as characteristic peaks of ZnS QDs, respectively [40,49]. Therefore it is believed that ZnO and ZnS QDs are co-existed in the B_ZnO QDs after synthesizing for 5 min with TAA. Absorption spectra for both Y_ZnO and G_ZnO QDs show similar behavior as like those of B_ZnO QDs. In case of NC_ZnO NPs, after synthesis with TAA the absorption peak at 290 nm instead of that at 266 nm is more dominantly observed. From the above results, it can be suggested that the absorption peaks of the B_, G_, Y_ZnO QDs, and NC_ZnO NPs related to ZnO rapidly decrease with the reaction for 5 to 10 min with TAA and finally vanish as the reaction proceeds. On the other hand, the absorption peaks related to ZnS QDs at 266 (Figure 3a–c) and 290 nm (Figure 3d) only remained clearly as the reaction proceeds. This can be interpreted as the consumption of the ZnO regardless of the particle size with the simultaneous formation of ZnS QDs and is in good agreement our above results.

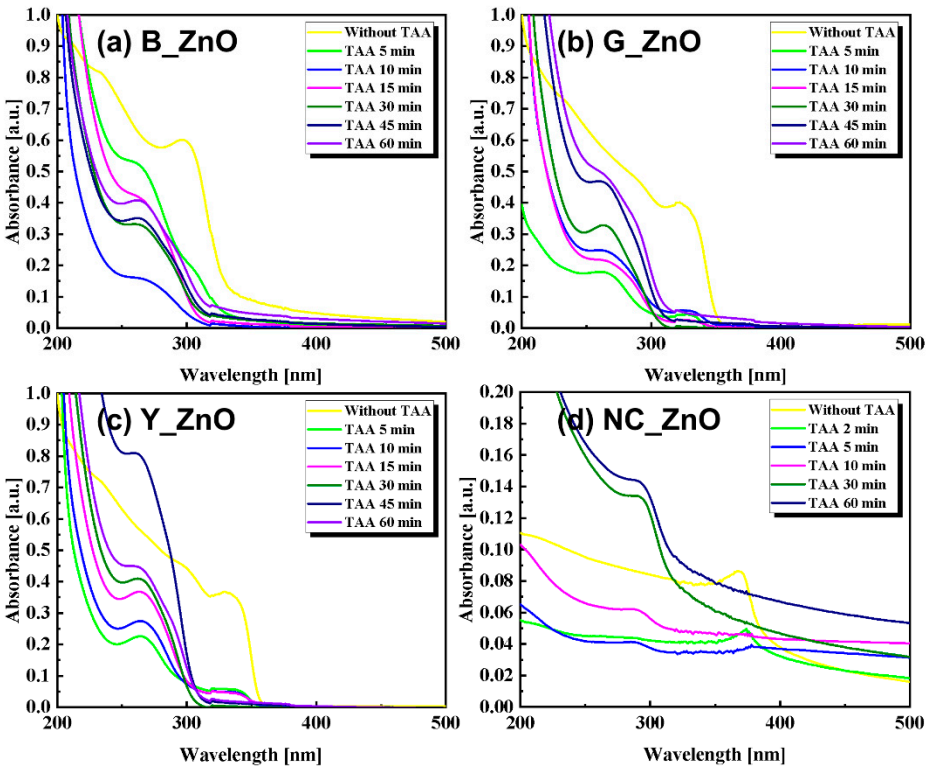


**Figure 3.** UV-Vis absorption spectra of size-controlled ZnO NPs synthesized with/without TAA measured at the indicated reaction times. (a) B_ZnO, (b) G_ZnO, (c) Y_ZnO QDs, and (d) NC_ZnO NPs.

PL spectra of ZnO NPs synthesizing at different reaction times with/without TAA are presented in Figure 4. For the optical mechanisms underlying their PL of ZnO NPs synthesized without TAA, the visible light emission is due to trap-induced defects on the surface and UV luminescence

Preprints (www.preprints.org) | NOT PEER-REVIEWED | Posted: 7 September 2023 doi:10.20944/preprints202309.0472.v1



corresponds to band-to-band emission [17,18]. The B_, G_, Y_ZnO QDs, and NC_ZnO NPs exhibited the PL peak centered at 466, 528, 538 and 378 nm, respectively. These PL results for B_, G_, and Y_ZnO QDs are good agreement with the occurrence of a blue-shift of PL wavelength as the particle size decreases. After reacting with TAA for 5 min, PL peaks of ZnO QDs were gradually disappeared, but instead new peak around 420 nm appeared clearly in all the samples. The PL peak at about 420 nm are well-known as characteristic of ZnS QDs [40,46,49]. In addition, the PL characteristics of visible luminescence corresponding to ZnO were significantly decreased for B_ZnO QDs, moderately decreased for G_, and Y_ZnO QDs, and slightly decreased for NC_ZnO. The PL characteristics of relatively small-sized B_ZnO QDs disappeared faster than other G_ and Y_ZnO QDs, which can be considered as the rapid consumption of smaller particles. In general, in most core/shell QDs, the PL property of the inner QDs could be improved by shelling with other materials which reduces the dangling bonds or structural defects distributed at the surface. In our cases, the expected enhancement of excitonic emission in ZnO NPs with the suppression of visible luminescence could not be seen as the increase of reaction time with TAA, but the improved PL intensity of ZnS QDs was clearly seen. After reacting with TAA for 60 minutes, only the PL characteristics of ZnS were observed in all the samples. This indicates that the reaction of ZnO NPs with TAA resulted in the formation of ZnS QDs rather than the surface shelling effect of ZnO NPs. The PL results are also in good agreement with our all results.

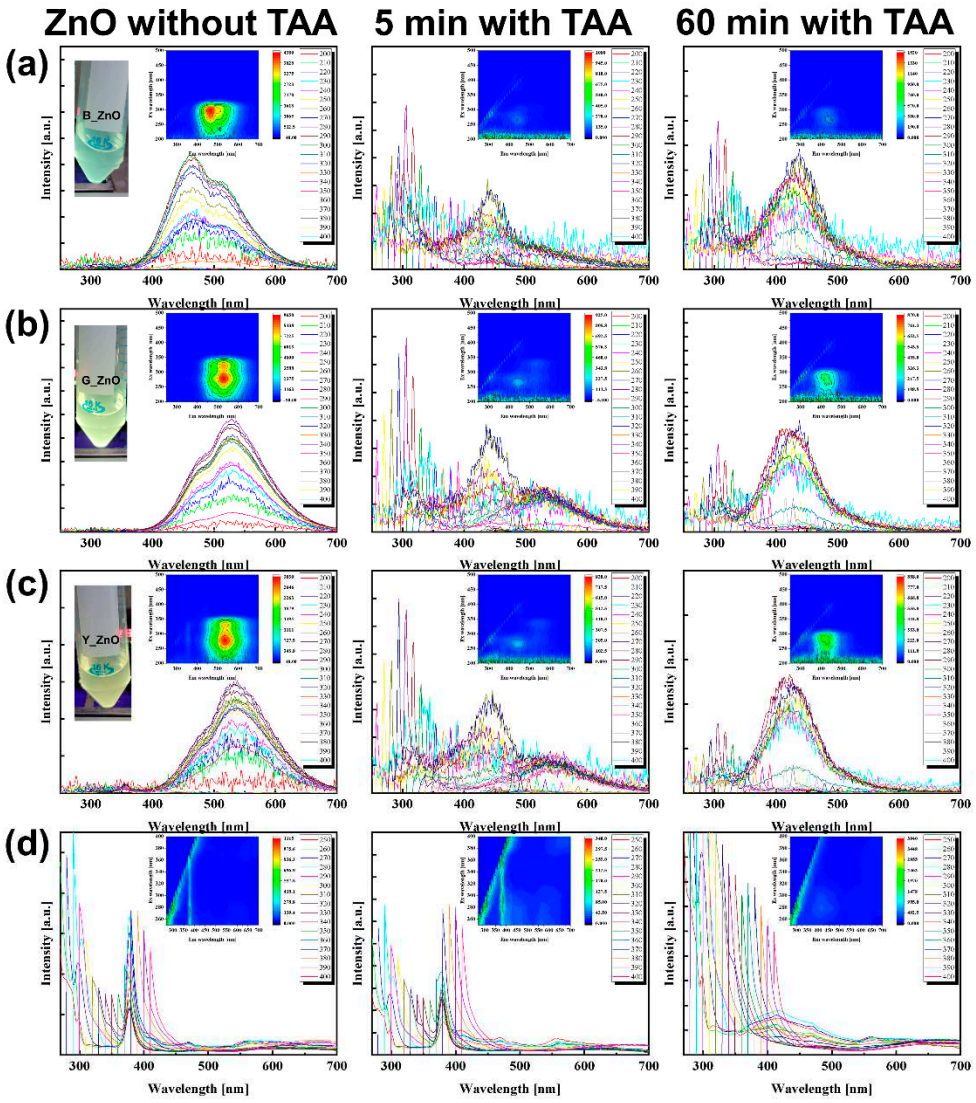


**Figure 4.** PL characteristics of size-controlled ZnO NPs synthesized with/without TAA measured at the indicated reaction times; Inset shows excitation and emission map for PL (Left: without TAA; Inset pictures show the luminescent images of ZnO NPs under UV excitation at 365 nm, middle:

synthesized for 5 min with TAA, right: synthesized for 60 min with TAA). (a) B_ZnO QDs, (b) G_ZnO QDs, (c) Y_ZnO QDs, and (d) NC_ZnO NPs.

## 4. Conclusions

In order to investigate the role of TAA in forming ZnS nanostructures from ZnO NPs, we synthesized size-controlled Y_, G_ and B_ZnO QDs by sol-gel method and a few tenth nm NC_ZnO NPs by hydrothermal method. In the reaction of all size-controlled ZnO NPs with TAA, the ZnO NPs were consumed and the ZnS QDs were formed, regardless of the sizes of preparation method of ZnO NPs. Our results enable a broader understanding of the synthetic mechanisms involved in the use of TAA as sulfur source in the formation of ZnO/ZnS nanocomposites.

**Author Contributions:** J.-S. Kim performed the experiment and analysis. J. Choi provided NC_ZnO NPs synthesized without TAA. J. Choi and W. K. Choi advised on the project, and J.-S. Kim and W. K. Choi wrote this manuscript.

**Data Availability Statement:** No new data were created or analyzed in this study. Data sharing does not apply to this article.

**Acknowledgments:** This work was supported by NRF (National Research Foundation of Korea) Grant funded by the Korean Government (NRF-2021-Global Ph.D. Fellowship Program) and the KIST Institutional Program (2E32242, 2V09706).

**Conflicts of Interest:** The authors declare no conflict of interest.

## References

1. Morkoç, H.; Özgür, Ü., Zinc Oxide. *Wiley-VCH Velag GmbH & Co. KGaA, Weinheim* **2009**.
2. Furno, E.; Bertazzi F.; Goano, Michele.; Ghione, G.; Bellotti, E., Hydrodynamic transport parameters of wurtzite ZnO from analytic- and full-band Monte Carlo simulation. *Solid-State Electron.* **2008**, *52*, 1796.
3. Park, J.-S.; Kyhm, J.; Kim, H. H.; Jeong, S.; Kang, J.; Lee, S.-e.; Lee, K.-T.; Park, K.; Barange, N.; Han, J.; Song, J. D.; Choi, W. K.; Han, I. K., Alternative Patterning Process for Realization of Large-Area, Full-Color, Active Quantum Dot Display. *Nano Lett.* **2016**, *16*, 6946.
4. Chao, M.-R.; Chang, Y.-Z.; Chen, J.-L., Hydrophilic ionic liquid-passivated CdTe quantum dots for mercury iondetection. *Biosens. Bioelectron.* **2013**, *42*, 397–402.
5. Tan, L; Kang, C; Xu, S; Tang, Y, Selective room temperature phosphorescence sensing of target protein using Mn-doped ZnS QDs-embedded molecularly imprinted polymer. *Biosens. Bioelectron.* **2013**, *48*, 216–223.
6. Zou, W.-s.; Qiao, J.-q.; Hu, X.; Ge, X.; Lian, H.-z., Synthesis in aqueous solution and characterisation of a new cobalt-doped ZnS quantum dot as a hybrid ratiometric chemosensor. *Anal. Chim. Acta* **2011**, *708*, 134–140.
7. Liu, J.; Wei, X.; Qu, Y.; Cao, J.; Chen, C.; Jiang, H., Aqueous synthesis and bio-imaging application of highly luminescent and low cytotoxicity $Mn^{2+}$-doped ZnSe nanocrystals. *Mater. Lett.* **2011**, *65*, 2139–2141.
8. Subash, B.; Krishnakumar, B.; Pandiyan, V.; Swaminathan, M.; Shanthi, M., An efficient nanostructured $Ag_2S$–ZnO for degradation of Acid Black 1 dye under day light illumination. Sep. *Purif. Technol.* **2012**, *96*, 204–213.
9. Liu, C.; Wang, Y.; Meng, D.; Yu, X.; Wang, Y.; Liu, J.; Lu, C.; Xu, K., Enhanced visible light photocatalytic performance of ZnO/ZnS/CuS ternary nanocomposites. *Mater. Lett.* **2014**, *122*, 197–200.
10. Nguyen, H. T.; Nguyen, N. D.; Lee, S., Application of solution-processed metal oxide layers as charge transport layers for CdSe/ZnS quantum-dot LEDs. *Nanotechnology* **2013**, *24*, 115201.
11. Janotti, A.; Walle, C. G. Van de, Fundamentals of zinc oxide as a semiconductor. *Rep. Prog. Phys.* **2009**, *72*, 126501.
12. Xiong, H.-M., ZnO Nanoparticles Applied to Bioimaging and Drug Delivery. *Adv. Mater.* **2013**, *37*, 5329–5335.
13. Matsuyama, K.; Ihsan, N.; Irie, K.; Mishima, K.; Okuyamam, T.; Mutom, H., Bioimaging application of highly luminescent silica-coated ZnO-nanoparticle quantum dots with biotin. *J. Colloid Interface Sci.* **2013**, *399*, 19–25.

14. Moussodia, R.-O.; Balan, L.; Merlin, C.; Mustin, C.; Schneider, R., Biocompatible and stable ZnO quantum dots generated by functionalization with siloxane-core PAMAM dendrons. *J. Mater. Chem.* **2010**, *20*, 1147–1155.
15. Manaia, E.B.; Kaminski, R.C.K.; Caetano, B.L.; Briois, V.; Chiavacci, L.A.; Bourgaux, C. Surface modified Mg-doped ZnO QDs for biological imaging. *Eur. J. Nanomed.* **2015**, *7*, 109–120.
16. Zhao, H.; Lv, P.; Huo, D.; Zhang, C.; Ding, Y.; Xu, P.; Hu, Y. Doxorubicin loaded chitosan-ZnO hybrid nanospheres combining cell imaging and cancer therapy. *RSC Adv.* **2015**, *5*, 60549–60551.
17. Ischenko, V.; Polarz, S.; Grote, D.; Stavarache, V.; Fink, K.; Driess, M., Zinc Oxide Nanoparticles with Defects, *Adv. Funct. Mater.* **2005**, *15*, 1945.
18. Gong, Y.; Andelman, T.; Neumark, G. F.; O'Brien, S.; Kuskovsky, I. L., Origin of defect-related green emission from ZnO nanoparticles: effect of surface modification, *Nanoscale Res. Lett.* **2007**, *2*, 297.
19. Asok, A.; Gandhia, M. N.; Kulkarni, A. R., Enhanced visible photoluminescence in ZnO quantum dots by promotion of oxygen vacancy formation, *Nanoscale*, **2012**, *4*, 4943–4946.
20. Zhang, L.; Yin, L.; Wang, C.; lun, N.; Qi, Y.; Xiang, D., Origin of Visible Photoluminescence of ZnO Quantum Dots: Defect-Dependent and Size-Dependent, *J. Phys. Chem. C*, **2010**, *114*, 9651–9658.
21. Kim, H. H.; Lee, H.; Kang, J. K.; Choi, W. K., Photoluminescence and Electron Paramagnetic Resonance Spectroscopy for Revealing Visible Emission of ZnO Quantum Dots. *Ann. Phys.* **2022**, *534*, 2100382.
22. Kim, H. H.; Park, S.; Lee, H.; Kang, J. K.; Choi, W. K., Blue-Light Emissive Type II ZnO@ 5-Amino-2-Naphthalene Sulfonic Acid Core–Shell Quantum Dots. *Adv. Photonics Res.* **2022**, *3*, 2100315.
23. Kim, H. H.; Lee, Y.; Lee, Y. J.; Jeong, J.; Yi, Y.; Park, C.; Yim, S.-Y.; Angadi, B.; Ko, K.-J.; Kang, J.-W.; Choi, W. K., Realization of excitation wavelength independent blue emission of ZnO quantum dots with intrinsic defects. *ACS Photonics* **2020**, *7*, 723–734.
24. Y. J. Lee,; H. H. Kim,; Y. J. Lee,; J. H. Kim,; H.-J. Choi,; Choi, W. K., Electron transport phenomena at the interface of Al electrode and heavily doped degenerate ZnO nanoparticles in quantum dot light emitting diode. *Nanotechnology* **2019**, *30*, 035207.
25. Kim, H. H.; Kumi, D. O.; Kim, K.; Park, D.; Yi, Y.; Cho, S. H.; Park, C.; Ntwaeaborwa, O. M.; Choi, W. K., Optimization of the electron transport in quantum dot light-emitting diodes by codoping ZnO with gallium (Ga) and magnesium (Mg). *RSC Adv.*, **2019**, *9*, 32066-32071.
26. Srinatha, N.; Angadi, B.; Son, D. I.; Choi, W. K., Structural and optical studies on spin coated ZnO-graphene conjugated thin films. *AIP Conf. Proc.* **2018**, *1953*, 100042.
27. Sharma, S.; Chawla, S. Enhanced UV emission in ZnO/ZnS core shell nanoparticles prepared by epitaxial growth in solution. *Electron. Mater. Lett.* **2013**, *9*, 267–271.
28. Luo, J.; Zhao, S.; Wu, P.; Zhang, K.; Peng, C.; Zheng, S. Synthesis and characterization of new Cd-doped ZnO/ZnS core-shell quantum dots with tunable and highly visible photoluminescence. *J. Mater. Chem. C* **2015**, *3*, 3391–3398.
29. Borgohain, R.; Das, R.; Mondal, B.; Yordsri, V.; Thanachayanont, C.; Baruah, S., ZnO/ZnS Core-Shell Nanostructures for Low-Concentration $NO_2$ Sensing at Room Temperature, *IEEE Sensors Journal* **2018**, *18*, 7203-7208.
30. Zhang, W.; Wang, S.; Wang, Y.; Zhu, Z.; Gao, X.; Yang, J.; Zhang, H. xin, ZnO@ZnS core/shell microrods with enhanced gas sensing properties, *RSC Advances* **2015**, *5*, 2620-2629.
31. Mun, Y.; Park, S.; Ko, H.; Lee, C.; Lee, S., $NO_2$ gas sensing properties of ZnO/ZnS core-shell nanowires, *Journal of the Korean Physical Society* **2013**, *63*, 1595-1600.
32. Qi, G.; Zhang, L.; Yuan, Z., Improved $H_2S$ gas sensing properties of ZnO nanorods decorated by a several nm ZnS thin layer, *Physical Chemistry Chemical Physics* **2014**, *16*, 13434-13439.
33. Park, S.; Kim, S.; Ko, H.; Lee, C., Light Assisted Room Temperature Ethanol Gas Sensing of ZnO–ZnS Nanowires, *Journal of nanoscience and nanotechnology* **2014**, *14*, 9025-9028.
34. Park, S.; Kim, S.; Ko, H.; Lee, C., Light-enhanced gas sensing of ZnS-core/ZnO-shell nanowires at room temperature, *Journal of Electroceramics* **2014**, *33*, 75-81.
35. Gao, P.; Wang, L.; Wang, Y.; Chen, Y.; Wang, X.; Zhang, G., Onepot hydrothermal synthesis of heterostructured ZnO/ZnS nanorod arrays with high ethanol sensing properties, *Chemistry–A European Journal* **2012**, *18*, 4681-4686.
36. Na, C. W.; Park, S.-Y.; Lee, J.-H., Punched ZnO nanobelt networks for highly sensitive gas sensors, *Sensors and Actuators B: Chemical* **2012**, *174*, 495-499.

37. Yu, X.-L.; Ji, H.-M.; Wang, H.-L.; Sun, J.; Du, X.-W., Synthesis and sensing properties of ZnO/ZnS nanocages, *Nanoscale research letters* **2010**, *5*, 644.
38. Yu, X.; Zhang, G.; Cao, H.; An, X.; Wang, Y.; Shu, Z.; An, X.; Hua, F., ZnO@ZnS hollow dumbbells–graphene composites as high-performance photocatalysts and alcohol sensors, *New Journal of Chemistry* **2012**, *36*, 2593-2598.
39. Reiss, P.; Protière, M.; Li, L. Core/Shell Semiconductor Nanocrystals. *Small* **2009**, *5*, 154–168.
40. Manaia, E. B.; Kaminski, R. C. K.; Caetano, B. L.; Magnani, M.; Meneau, F.; Rochet, A.; Santilli, C. V.; Briois, V.; Bourgaux, C.; Chiavacci L. A., The Critical Role of Thioacetamide Concentration in the Formation of ZnO/ZnS Heterostructures by Sol-Gel Process. *Nanomaterials* **2018**, *8*, 55.
41. Kim, J.-S.; Kang, B.-H.; Jeong, H.-M.; Kim, S.-W.; Xu, B.; Kang, S.-W., Quantum dot light emitting diodes using size-controlled ZnO NPs. *Curr. Appl. Phys.* **2018**, *18*, 681-685.
42. Son, D., Kwon, B., Park, D. et al. Emissive ZnO–graphene quantum dots for white-light-emitting diodes. *Nature Nanotech* **2012,** *7*, 465–471.
43. Briois, V.; Giorgetti, Ch.; Baudelet, F.; Blanchandin, S.; Tokumoto, M. S.; Pulcinelli, S. H.; Santilli, C. V., Dynamical Study of ZnO Nanocrystal and Zn-HDS Layered Basic Zinc Acetate Formation from Sol-Gel Route. *J. Phys. Chem. C* **2007**, *111*, 3253.
44. Spanhel, L., Colloidal ZnO nanostructures and functional coatings: A survey. *J Sol-Gel Sci Techn.* **2006**, *39*, 7.
45. Segets, D.; Marczak, R.; Schäfer, S.; Paula, C.; Gnichwitz, J.-F.; Hirsch, A.; Peukert, W., Experimental and Theoretical Studies of the Colloidal Stability of Nanoparticles−A General Interpretation Based on Stability Maps. *ACS Nano* **2011**, *5*, 4658–4669.
46. Wang, F.; Liu, J.; Wang, Z.; Lin, A.-J.; Luo, H.; Yu, X., Interfacial Heterostructure Phenomena of Highly Luminescent ZnS/ZnO Quantum Dots. *J. Electrochem. Soc.* **2011**, *158*, H30.
47. West, A. R., Solid State Chemistry and Its Applications, 2nd ed. *John Wiley and Sons* **1992**, ISBN 978-1-119-94294-8.
48. Meulenkamp, E. A., Synthesis and Growth of ZnO Nanoparticles. *J. Phys. Chem. B* **1998**, *102*, 5566-5572.
49. Mehta, S.K.; Kumar, S.; Chaudhary, S.; Bhasin, K.K.; Gradzielski, M., Evolution of ZnS Nanoparticles via Facile CTAB Aqueous Micellar Solution Route: A Study on Controlling Parameters. *Nanoscale Res. Lett.* **2009**, *4*, 17.